Journal of Catalysis **186,** 458–469 (1999)
Article ID jcat.1999.2564, available online at http://www.idealibrary.com on IDEAL®

Comparative Study of Au/TiO_2 and Au/ZrO_2 Catalysts for Low-Temperature CO Oxidation

Jan-Dierk Grunwaldt,[1] Marek Maciejewski, Olav Sven Becker,[2] Patrizia Fabrizioli, and Alfons Baiker[3]

Laboratory of Technical Chemistry, Swiss Federal Institute of Technology, ETH-Zentrum, CH-8092 Zürich, Switzerland

Received March 29, 1999; revised May 10, 1999; accepted May 20, 1999

Gold catalysts for low-temperature CO oxidation were prepared by immobilizing gold colloids of about 2 nm size on TiO_2 and ZrO_2 in aqueous solution. The gold particles nearly retained their size after immobilization on both supports. Slight sintering was observed by X-ray diffraction and high-resolution transmission electron microscopy after calcination at 673 K. Some of the gold particles on ZrO_2 showed hexagonal symmetry with close-packed Au(111) surfaces. X-ray photoelectron spectroscopy investigations indicated that the gold was in a metallic state. Whereas gold particles on TiO_2 showed CO conversion directly after preparation and drying, significant activity of gold on ZrO_2 was only observed after calcination in air. CO adsorption was reversible on all catalysts and weaker on the most active catalysts, as shown by diffuse reflectance Fourier transform infrared spectroscopy (DRIFTS) and pulse thermal analysis. Probing of the gold sites by CO adsorption revealed the existence of different gold sites in these catalysts. Step/kink sites (2111–2123 cm^{-1}) and positively polarized gold sites (2128–2135 cm^{-1}) were identified on uncalcined and *in situ* calcined gold catalysts. The number of low-coordinated gold sites was much higher on TiO_2, whereas on ZrO_2 more positively polarized gold atoms were found. This behaviour was traced to the shape of the gold particles, which affects the number of low-coordinated gold atoms and is dependent on support and treatment. *In situ* treatment in oxygen led to a temporarily inactive catalyst with additional bands in the DRIFTS spectrum in the 2000–2400 cm^{-1} region, stemming from CO adsorbed on positively polarized gold sites (2130–2150 cm^{-1}) and on the support (2180–2200 cm^{-1}), and from molecularly adsorbed CO_2 (2353 cm^{-1}). No bands arising from CO on low-coordinated, metallic gold sites were identified in that case.

1. INTRODUCTION

In contrast to the bulk metal, which is known to be rather inert in CO oxidation (e.g., (1, 2)), gold nanoparticles deposited on selected metal oxides often exhibit high and unusual activity. In particular, recent research has demonstrated that highly dispersed gold supported on reducible oxides such as TiO_2 (2–5), Fe_2O_3 (3, 4, 6), Co_3O_4 (3, 6), and NiO (6) is very active in low-temperature CO oxidation.

The reason for higher activity of the more dispersed clusters is still under discussion. Valden *et al.* (7, 8) recently concluded from a model catalyst study that CO oxidation on gold is related to a quantum size effect. Haruta and coworkers (9, 10), however, showed that the interface and the support play a significant role. Bollinger and Vannice (2) reported furthermore that the deposition of TiO_x overlayers onto inactive gold particles produced highly active catalyst, which argues against a quantum size effect.

To gain a more detailed insight into the different factors controlling the activity of gold catalysts, the development of flat and powdered model systems was started in our group (5, 11–13), indicating that particle size and support play a significant role. Moreover, we concluded that oxygen adsorption and activation is the crucial step in CO oxidation and showed that colloids of about 2 nm in size supported on zirconia and titania are active for CO oxidation. The colloidal route has the advantage that the gold particle size is virtually established before deposition (5, 14) and thus less dependent on the support than with other methods. The gold particles prepared by deposition–precipitation or coprecipitation are formed by heating to higher temperatures (2, 3, 6). Also the use of $[Au(PPh_3)](NO_3)$ as precursor requires higher temperatures (4, 15). Strong sintering is observed in the case of oxides and can only be prevented if as-precipitated hydroxides are used. Visco *et al.* used as precipitated hydroxides for the preparation of active Au/Fe_2O_3 catalysts (16). Recently chemical vapour deposition of dimethylgold(III)β-diketone was also used by Okumara (17). However, temperatures higher than 573 K are required for burning off the ligand residues and form small gold particles (17).

Therefore, the preparation of gold catalysts with small gold colloids (around 2 nm in size) is a useful strategy to gain more detailed understanding of the influence of particle size, support, and calcination temperature on CO oxidation activity. Gold catalysts with titania as support are

[1] Present address: Haldor Topsøe A/S Research Laboratories, Nymøllevej 55, DK-2800 Lyngby, Denmark.

[2] Institute for Inorganic Chemistry, University of Zürich, Winterthurer Str. 190, CH-8057 Zürich, Switzerland.

[3] Corresponding author. Fax: +41 1 632 11 63. E-mail: baiker@tech.chem.ethz.ch.

0021-9517/99 $30.00

reported to be superior to those with zirconia as support (e.g., (3, 18)). The present study aims at elucidating the differences of these catalysts. In order to gain deeper insight into the properties of gold sites exposed on the surface of Au/TiO_2 and Au/ZrO_2 catalysts, we carried out DRIFTS studies using CO as probe molecule at different stages of the catalytic investigations.

2. EXPERIMENTAL

2.1. Catalyst Preparation

Au/TiO_2 (1.7 wt% Au) and Au/ZrO_2 (1.7 wt% Au) were prepared by reduction of $HAuCl_4$ with tetrakis (hydroxymethyl) phosphonium chloride (THPC), adsorption of the as-formed colloids at pH 2 on the corresponding oxides, TiO_2 (P25, Degussa, $S_{BET} = 60$ m^2/g) and ZrO_2 (Degussa, $S_{BET} = 40$ m^2/g), and subsequent drying for 15 h at 323 K under vacuum as described in Ref. (5). For *ex situ* calcination the raw catalysts were heated in air with 4 K/min to 673 K and cooled after 1 h in Ar. The samples used are listed in Table 1. For some experiments (XRD, thermal analysis) similarly prepared higher loaded catalysts (16.6 wt% Au) were used.

2.2. Catalyst Characterization

Catalytic tests. Steady-state catalytic tests were carried out in a continuous flow fixed-bed microreactor as described in detail in Ref. (5). The powder was fixed between glass wool plugs in a 6 mm i.d. quartz glass reactor tube. Experiments in the temperature range 250–450 K and at atmospheric pressure were performed using 200 mg catalyst. Standard experiments were performed using a CO feed rate of 2.5×10^{-7} mol s^{-1} g cat^{-1}. The gas hourly space velocity amounted to ca. 12000 h^{-1} (flow rate per total bed volume). Kinetic data were taken after 20 min on stream at specified conditions. Products were analysed by either gas chromatography or an FTIR spectrometer with heatable gas cell.

High resolution transmission electron microscopy (HRTEM). HRTEM investigations were carried out using a Phillips CM 30 ST electron microscope with CeB6-cathode and a Jeol 2010 electron microscope with LaB6-cathode at accelerating voltages of 300 and 200 kV, respectively.

X-ray diffraction (XRD). XRD of the supported gold particles was performed on a Siemens D 5000 powder X-ray diffractometer using Ni-filtered Cu $K\alpha$ radiation at 45 kV and 35 mA.

X-ray photoelectron spectroscopy (XPS). The surface composition and oxidation state of the surface atoms was examined by XPS using a Leybold Heraeus LHS 11 MCD instrument. Mg $K\alpha$ radiation was used to excite photoelectrons, which were analysed with the analyser, operated at 150 eV pass energy at an energy scale calibrated versus Au $4f_{7/2}$ at 84.0 eV. The surface composition of the samples was determined from the peak areas of the corresponding lines using a Shirley type background and empirical cross section factors for XPS (19, 20).

Thermoanalytical investigations. Differential scanning calorimetry (DSC) and thermogravimetry (TG) were carried out using a Netzsch STA 409 thermoanalyser which was connected to a valve device enabling pulse thermal analysis (PTA) (21, 22). This setup allowed the injection of small volumes (0.25–1.0 ml) of required gas into an Ar carrier flow during the thermoanalytical experiments. Evolving gases were monitored using a Balzers QMG 420 quadrupole mass spectrometer, which was connected to the thermoanalyser by a heated capillary.

Nitrogen adsorption. BET surface areas (S_{BET}), mean cylindrical pore diameters ($\langle dp \rangle$), and specific adsorption pore volumes (V_p) were obtained by physisorption of N_2 at 77 K using a Micromeritics ASAP 2000 instrument. Prior to measurement, the samples were degassed to 0.1 Pa at 363 K. The S_{BET} areas were calculated in a relative pressure range $0.05 < p/p_0 < 0.2$ assuming a cross-sectional area of 0.162 nm^2 for the N_2 molecule (23).

Diffuse reflectance infrared Fourier transform spectroscopy (DRIFTS). The CO adsorption and the CO oxidation reaction were monitored *in situ* by DRIFTS under defined reaction conditions. Spectra were recorded on an FTIR instrument (Perkin Elmer, Model 2000) containing a diffuse reflection unit and a controlled environmental chamber (both Spectra-Tech) equipped with two CaF_2 windows (permeable >1000 cm^{-1}). The powdered sample was mounted on a ceramic frit (Al_2O_3) which could be heated to elevated temperature (here 573 K) via a PID controller (Tecon 501). Prior to measurements, the catalyst samples were outgassed in an Ar gas stream (Pangas, 99.999%; 50 ml/min) for more than 2 h at 298 K, as in the case of activity measurements. *In situ* calcination was performed with O_2 in Ar (40% O_2, Pangas, 99.999%, flow rate 50 ml/min). All further experiments were performed with a gas stream of 6 ml/min using the following gas

TABLE 1

Overview of Catalysts Investigated

Catalyst	Treatment
Dried Au/TiO_2 (1.7 wt% Au)	Dried at 323 K in vacuum
Dried Au/ZrO_2 (1.7 wt% Au)	Dried at 323 K in vacuum
Activated Au/TiO_2 (1.7 wt% Au)	Calcined *ex situ* at 673 K in air
Activated Au/ZrO_2 (1.7 wt% Au)	Calcined *ex situ* at 673 K in air
TiO_2	Reference sample, Degussa TiO_2 P25
ZrO_2	Reference sample, Degussa ZrO_2

mixtures: CO adsorption was carried out with CO in He (5260 ppm CO, Pangas, 99.997%), followed by desorption in pure Ar (Pangas) or desorption/reaction under oxidative conditions in O_2 in He (5000 ppm O_2, Pangas, 99.999%), and finally reaction conditions were mimicked using a 1:1 mixture of CO in He (5260 ppm CO) and O_2 in He (5000 ppm). The gases were dried in a cooling trap (CO_2/isopropanol cooling mixture), and the gas flow was adjusted by mass flow controllers (Brooks, Model 5850 TR).

3. RESULTS

3.1. Structural Characterization

The untreated catalysts (dried at 323 K in vacuum for 15 h, compare Ref. (5, 12)) were characterized with HRTEM, XPS, and XRD. HRTEM images of the Au/TiO_2 (1.7% loading) and Au/ZrO_2 (1.7% loading) catalysts, used for this study, were very similar to those used in a previous study (5); therefore, only two enlargements are depicted in Figs. 1a and 1b. The mean particle size for gold dispersed

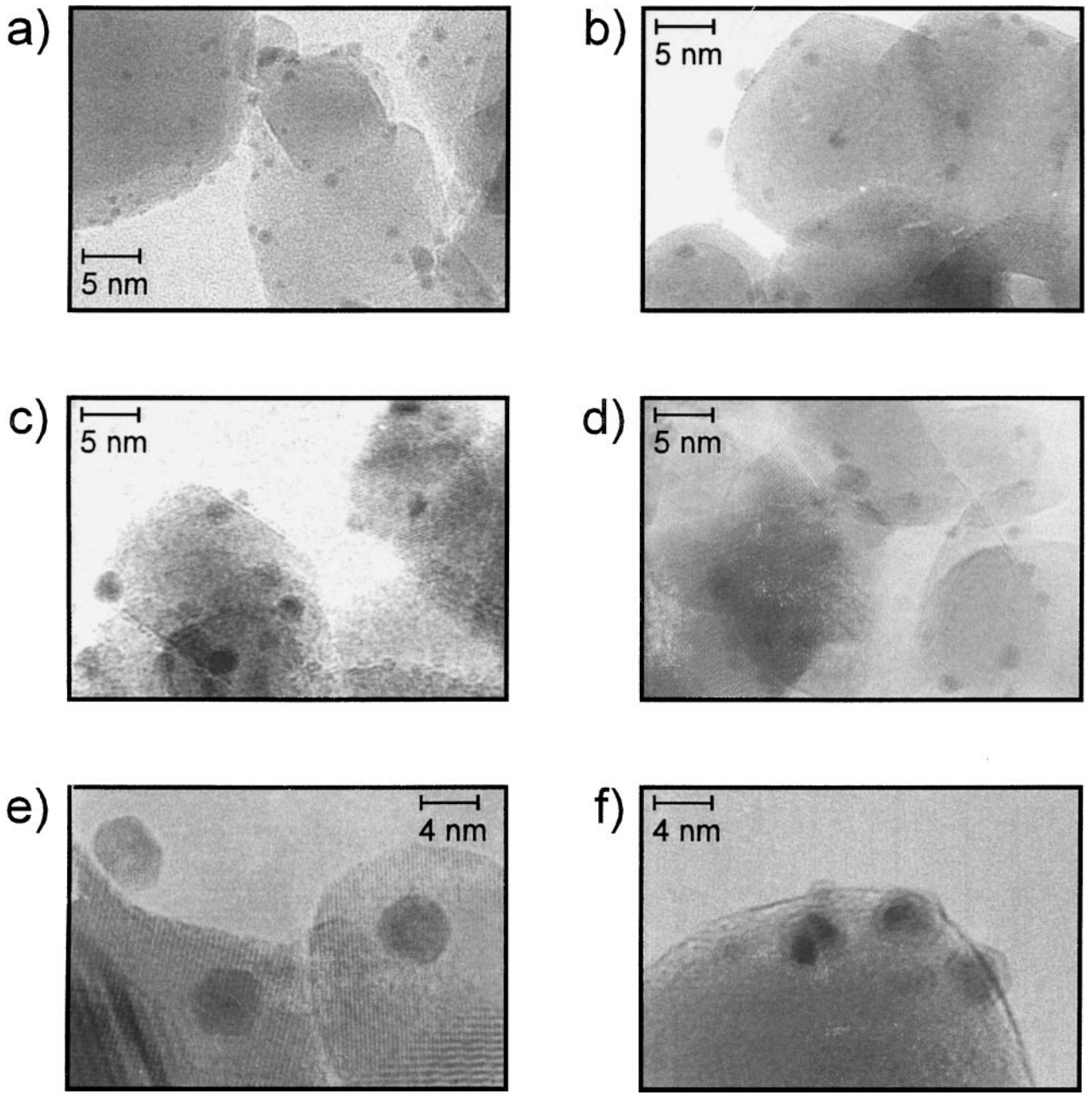

FIG. 1. HRTEM investigations of Au/TiO_2 and Au/ZrO_2 catalysts (1.7 wt% Au) after drying at 323 K under vacuum, (a) Au/TiO_2, (b) Au/ZrO_2, and after activation at 673 K in oxygen, (c) Au/TiO_2, (d) Au/ZrO_2. Parts (e) and (f) show selected regions of Au/ZrO_2 after activation at 673 K in oxygen.

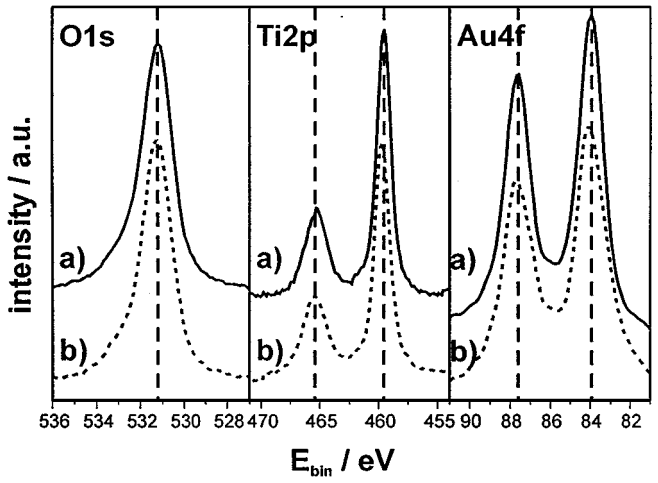

FIG. 2. XP-spectra of the O 1*s*, Ti 2*p*, and Au 4*f* region of Au/TiO_2 (1.7 wt% Au) (a) before (surface composition, 4.0 at% C, 71.0 at% O, 24.3 at% Ti, 0.7 at% Au) and (b) after activation at 673 K in oxygen (surface composition, 5.3 at% C, 67.8 at% O, 26.3 at% Ti, 0.7 at% Au).

on zirconia is about 2 nm, and it is slightly less (1.5–2 nm) on titania. The shape of the particles depends on the support (near spherical on TiO_2, more flat on ZrO_2). Typical Au(111) fringes could be resolved only on very few particles, probably because the particle size was too small and the contrast not as good as with gold colloids from the solution directly supported on the carbon grid. In this case distinct Au(111) fringes were found, especially for large gold aggregates aged for several days or weeks. XRD revealed that due to small particle size no distinct reflexes of gold could be identified.

XPS-analysis showed that the gold dispersion was similar on both catalysts (5) and that the samples contained traces of phosphorous, whereas no sodium was detectable. More detailed analysis with deposition of gold colloids on MeO_2/Au(111)/mica plates ($MeO_2 = TiO_2$, ZrO_2) uncovered that in acidic solution, as used in this study, the amount of adsorbed phosphorous species and sodium is lowered compared to solutions with higher pH (11). Figure 2a depicts the XP spectra of the Au/TiO_2 sample before calcination. The detected Au 4*f* peaks did not show any appreciable shift in the binding energies from those of bulk gold, indicating that the gold particles were in metallic state under high-vacuum conditions. Also on Au/ZrO_2 the gold particles were in metallic state. The surface composition of Au/ZrO_2 determined by XPS has been reported in Ref. (5).

TA-MS indicated that carbon impurities evolved from the catalysts around 500 K ($m/z = 41, 43, 56$) and some water around 373 K. At 650–750 K a strong mass spectrometric signal due to carbon dioxide evolution (shown for Au/TiO_2 in Fig. 3) was observed. No indication for sintering of the gold was noticeable up to 700 K. According to calculations, sintering is expected to occur around 570 K for isolated clusters of about 2 nm in size (24).

HRTEM images of the Au/TiO_2 (1.7 wt% Au) and Au/ZrO_2 (1.7 wt% Au) catalysts, after calcination at 673 K and use for room temperature CO oxidation, are shown in Figs. 1c and 1d. TiO_2-supported particles remained spherical and some of the images indicate that they were well attached to the support. In contrast, on Au/ZrO_2 some of the particles grew (to 4–6 nm) or changed their shape (indicating hexagonal symmetry, as shown in Figs. 1e and 1f). Furthermore, the contrast of the images was significantly lower than in the uncalcined samples.

XRD with highly loaded Au/TiO_2 and Au/ZrO_2 (16.6 wt% Au) showed no significant increase of the crystallite size during heating to 673 K. Only samples heated in air to temperatures higher than 873 K (ramp rate 10 K/min) resulted in significant particle size increase. The drastic increase in crystallite size compared to the uncalcined sample is shown in Fig. 4 for the Au/TiO_2 catalyst. Distinct reflections are resolved at $2\theta = 38.2^\circ$ (111), 44.4° (200), and 64.6° (220) (Fig. 4c). The calculated crystallite size is 7–8 nm.

Catalytic tests with highly loaded gold catalysts, calcined at different temperatures, showed that CO oxidation increased with increasing calcination temperatures and decreased again upon sintering. This is illustrated in Fig. 5,

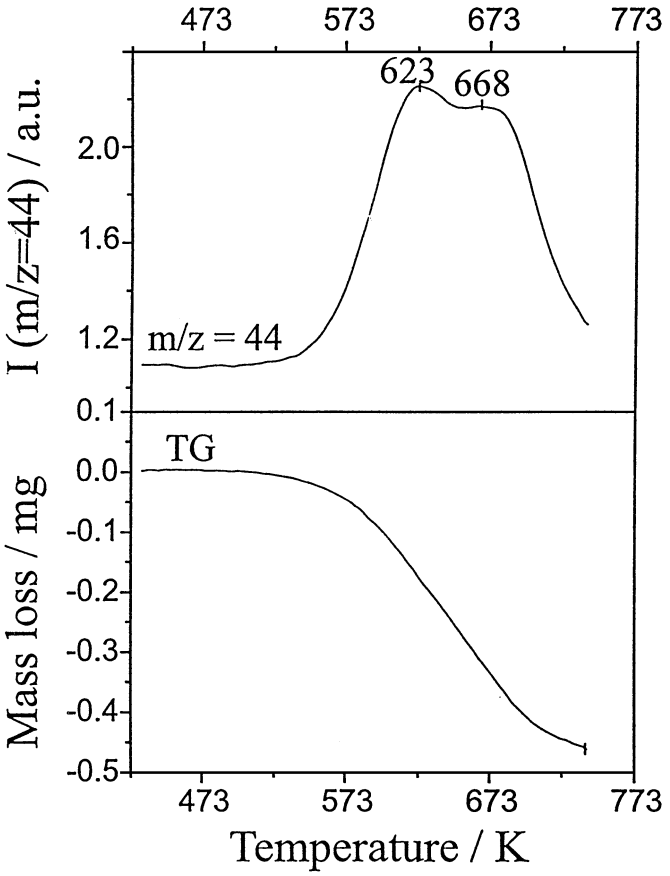

FIG. 3. Mass loss and evolution of CO_2 ($m/z = 44$) from highly loaded Au/TiO_2 catalyst (16.6 wt%) during heating under oxygen to 743 K.

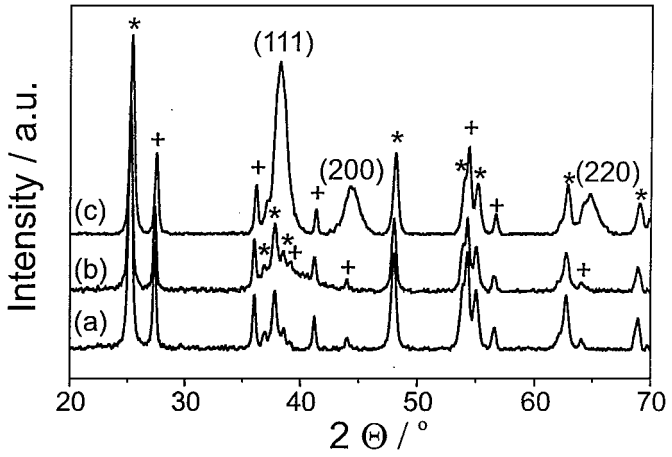

FIG. 4. XRD patterns of (a) support, (b) highly loaded uncalcined Au/TiO_2 (16.6 wt%), and (c) calcined sample heated to 900 K (ramp rate 10 K/min). Plus signs denote reflections of rutile; asterisks denote anatase.

which shows the evolution of CO_2 as a result of CO pulsing over Au/TiO_2 calcined at different temperatures. A similar behaviour was found for the corresponding Au/ZrO_2 catalyst, however, at lower activity (compare Section 3.2.).

XP-spectra of Au/TiO_2 (Fig. 2) and Au/ZrO_2 (not shown) of the Au 4*f*, Ti 2*p*, and O 1*s* regions revealed that before and after (*ex situ*) calcination the location of the peaks is rather similar. However, it should be noted that the Au $4f_{7/2}$ peaks were broader in the calcined catalyst. This could be due to either partial oxidation or charging of the gold particles. Charging is unlikely because Ti 2*p* and O 1*s* peaks did not show broadening. For gold oxides a shift of 2.0–2.5 eV is expected (25). Stronger oxidized gold sites, as reported by Epling *et al.* (26) on Au/Fe_2O_3, were not observed. BET areas of the catalysts after calcination were 42 m^2/g for Au/TiO_2, and 32 $m^2\ g^{-1}$ for Au/ZrO_2.

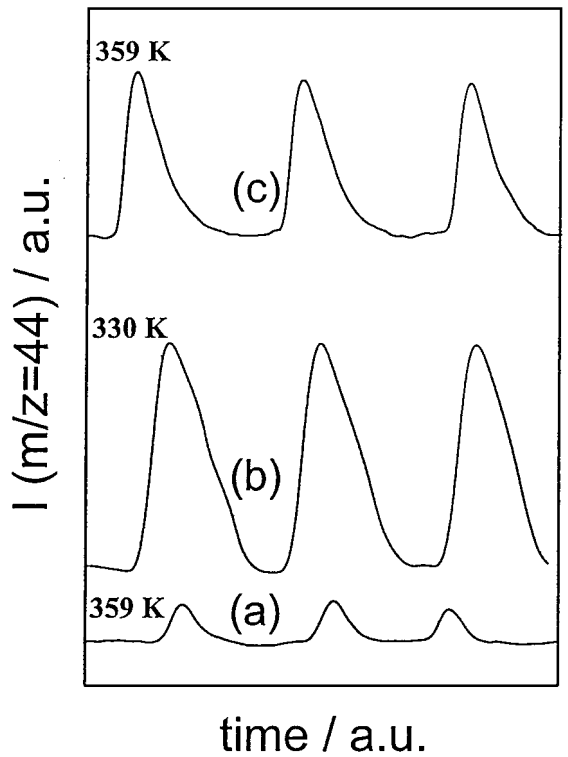

FIG. 5. Evolution of CO_2 ($m/z = 44$) resulting from CO pulses over Au/TiO_2 (16.6 wt%) at 330 and 359 K. Sample activated in O_2 at (a) 408, (b) 743, and (c) 800 K. Duration of measurement is about 40 min.

3.2. *Catalytic Behaviour in CO Oxidation*

The catalytic activities at room temperature of the Au/TiO_2 and Au/ZrO_2 catalysts, used throughout this work, are listed in Table 2. Note that a 1 : 1 mixture of CO and O_2 was used as, e.g., in Refs. (5, 18). Interestingly, the uncalcined Au/TiO_2 catalyst exhibited high activity at room temperature, whereas the Au/ZrO_2 catalyst did not show any activity under these conditions. DRIFTS (see Section 3.3) independently supports this observation. The Au/TiO_2 catalyst could be activated by heating in the reaction mixture. Figure 6 shows this behaviour of the uncalcined Au/TiO_2 catalyst in more detail.

After calcination Au/ZrO_2 catalysts were more active, although some of the gold particles sintered. However, the activity was significantly lower compared to the calcined Au/TiO_2 catalyst. The temperature for 50% CO conversion was about 373 K for Au/ZrO_2 and 285 K for Au/TiO_2. As stated in a previous publication (5) the activity of the Au/ZrO_2 catalyst resembled that of a coprecipitated Au/ZrO_2 catalyst under the same reaction conditions (18). It is noteworthy to mention that the Au/TiO_2 catalyst seems to be more active than a catalyst recently prepared via gold colloids by Haruta *et al.* (27). Table 2 shows that the catalytic activity directly after activation (heating in air to 673 K,

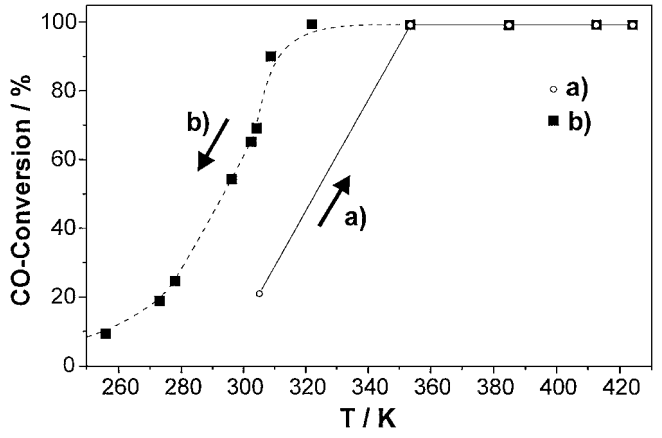

FIG. 6. Influence of temperature on CO conversion over uncalcined Au/TiO_2 (1.7 wt% Au): (a) heating cycle, (b) cooling cycle (value at 304 K taken after 1 day). Conditions: 200 mg catalyst, total flow rate 30 $cm^3\ min^{-1}$, 2500 ppm O_2, 2500 ppm CO, balance nitrogen.

TABLE 2

Activity of Au/TiO_2 and Au/ZrO_2 Catalysts under the Conditions Specified in the Text after Different Treatments

Sample	History of the sample	Temperature	Conversion
Au/TiO_2 (1.7 wt%)	Uncalcined, dried for 15 h at 323 K	304 K	21%
Au/ZrO_2 (1.7 wt%)	Uncalcined, dried for 15 h at 323 K	300 K	<1%
Au/TiO_2 (1.7 wt%)	Uncalcined, heated in reaction mixture to 423 K	304 K	68%
Au/TiO_2 (1.7 wt%)	Freshly calcined at 673 K	300 K	100%
Au/TiO_2 (1.7 wt%)	Calcined at 673 K, steady state	300 K	70%
Au/ZrO_2 (1.7 wt%)	Freshly calcined at 673 K	300 K	15%
Au/ZrO_2 (1.7 wt%)	Calcined at 673 K, steady state	300 K	10%

cooling in Ar) was slightly higher than when reaching steady state.

3.3. *DRIFTS Experiments*

DRIFTS was used to study the adsorption of CO on uncalcined, *ex situ*, and *in situ* calcined catalysts under different conditions (CO atmosphere, CO/O_2 mixture, desorption in Ar and O_2) to gain further insight into the exposed Au-sites. For this purpose the vibrational bands were assigned on the basis of adsorption on pure ZrO_2 and TiO_2 supports and with the help of bands reported in the literature (28–32).

3.3.1. Spectra of catalysts during in situ calcination. Typical *in situ* spectra during calcination in an oxygen stream (40% O_2 in Ar) are shown in Figs. 7a (Au/TiO_2) and 7b (Au/ZrO_2). Bands are located between 1000 and 1650 cm^{-1}, as well as in the 3600–3700 cm^{-1} region. According to previous results (18), the band around 3674 cm^{-1} is assigned to bridging OH-groups, the terminal OH-groups probably being blocked by the formation of a surface carbonate. Hence, in the carbonyl stretching region, monodentate carbonate (1350–1400 cm^{-1}, 1400–1450 cm^{-1}) and bidentate carbonate (1220–1300 cm^{-1}, Fig. 7b) were found. The band around 1623 cm^{-1} (Fig. 7b) is due to a δ(OH)-vibration of adsorbed water and decreased during heating in the cell. Both monodentate and bidentate carbonate decomposed at higher temperatures (decrease of some bands in the carbonyl stretching region), which is also supported by thermal analysis (Fig. 3).

3.3.2. CO adsorption and desorption in argon. In order to discriminate between the adsorption properties of the surface Au atoms and the support materials, CO adsorption was first studied on pure TiO_2 and ZrO_2. The uncalcined support materials did not show any pronounced IR bands in the region 2000–2100 cm^{-1}, when exposed to a CO flow. Only the doublet of free CO, located around 2149 cm^{-1} was found (not shown). After *in situ* calcination of the sample in oxygen at 673 K, a new band at 2187 cm^{-1} developed, when the gas flow was switched to 5200 ppm CO in He at room temperature (not shown). This band disappeared within 2–4 min if the flow was changed to Ar. The corresponding zirconia sample behaved similarly, showing a band around 2190 cm^{-1} only after *in situ* heating. These bands correspond to CO adsorbed on Ti^{4+} and Zr^{4+} centres, respectively (cf. Table 3).

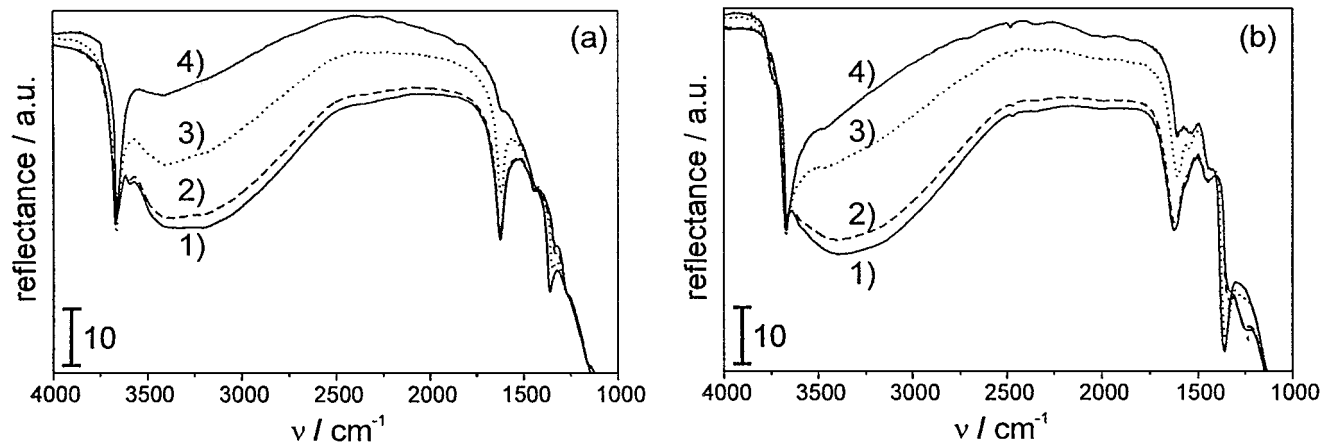

FIG. 7. DRIFT spectra of gold catalysts at different temperatures in an oxygen stream (40% O_2/Ar), (a) Au/TiO_2 and (b) Au/ZrO_2, at (1) room temperature, and at (2) 373, (3) 473, and (4) 573 K.

TABLE 3

CO- and CO_2-species Detected on Au/TiO_2 and Au/ZrO_2 in the Region 2000 cm^{-1}–2400 cm^{-1}

Observed vibration bands (in cm^{-1})	Gold sites on which CO/CO_2 species are adsorbed	Reference
2064	Bridged CO on gold sites	(2)
2111–2123	CO on gold sites	(28, 30)
2128–2135	CO on positively polarized gold sites	(29, 30)
2149, doublet	Free CO	
2187–2189	CO on Ti^{4+}	(31)
2180–2197	CO on Zr^{4+}	(31)
2353	Adsorbed CO_2	(30, 32)

Figures 8–10 show the carbonyl stretching region (2000–2400 cm^{-1}) of the desorption of CO in an argon stream on uncalcined Au/TiO_2 (Fig. 8a) and Au/ZrO_2 (Fig. 8b), on *ex situ* calcined and catalytically active Au/TiO_2 (Fig. 9a) and Au/ZrO_2 (Fig. 9b), and *in situ* calcined Au/TiO_2 (Fig. 10a) and Au/ZrO_2 (Fig. 10b). Upon adsorption of CO on Au/TiO_2 and Au/ZrO_2 catalysts, strong bands developed between 2110 and 2140 cm^{-1}. In all these and further IR spectra, no correction has been made for free CO and CO_2. The adsorption of CO on the gold catalysts was reversible, and faster for the active catalysts.

The adsorption of CO on uncalcined Au/TiO_2 (Fig. 8a) led to a strong band at 2112 cm^{-1} with a small shoulder at 2128 cm^{-1}. The shoulder was more pronounced in the beginning of the CO adsorption process. At that stage also some CO_2 desorbed. During desorption of CO, which lasted longer than on the pure supports, the bands shifted to higher wavenumbers. This "blue shift" could also be observed during the adsorption and if different partial pressures of CO were used, similar to reports on other catalysts (2, 30).

The uncalcined Au/ZrO_2 catalyst (Fig. 8a) showed similar features: Bands at about 2119 and 2129 cm^{-1} appeared upon CO adsorption, and the band at higher frequencies was more pronounced compared to Au/TiO_2. The desorption from the catalyst proceeded more slowly compared to the corresponding titania supported material. Similarly to Au/TiO_2 a blue shift for the lower frequency band was observed.

The investigation of CO adsorption on *ex situ* calcined and used catalysts (Fig. 9) revealed again a typical band of CO which developed around 2111 (Au/TiO_2) and 2119 cm^{-1} (Au/ZrO_2). The bands shifted to 2118 and 2123 cm^{-1} during desorption, which proceeded more quickly in both cases compared to the uncalcined catalysts. When CO concentration was lowered from 5200 to 1700 ppm the band shifted from 2111 to 2114 cm^{-1} for Au/TiO_2, and from 2119 to 2122 cm^{-1} for Au/ZrO_2 (not shown). Again, the samples showed a shoulder around 2128 cm^{-1} which was more pronounced during desorption (Fig. 9) or in the beginning of the adsorption process. For Au/ZrO_2 the shoulder shifted to about 2134 cm^{-1} during desorption and was more pronounced than for the Au/TiO_2 catalyst.

After *in situ* calcination of the catalyst at 573 K, the DRIFT spectra of CO desorption showed some additional features, as seen in Figs. 10a and 10b. In the CO region only one signal was detected at 2135 (Au/ZrO_2, small shoulder) and 2139 cm^{-1} (Au/TiO_2). No band developed between 2110 and 2120 cm^{-1}, as found for the catalysts which had been calcined *ex situ* in air at 673 K (Fig. 9). However, additional features arose at 2196 (Au/ZrO_2) and 2189 cm^{-1} (Au/TiO_2), respectively, due to CO adsorption on the support materials (compare results on pure supports at the beginning of this section). For both catalysts a strong band developed at 2353 cm^{-1}. The band was strongest after 4 min exposure to the argon flux and subsequently

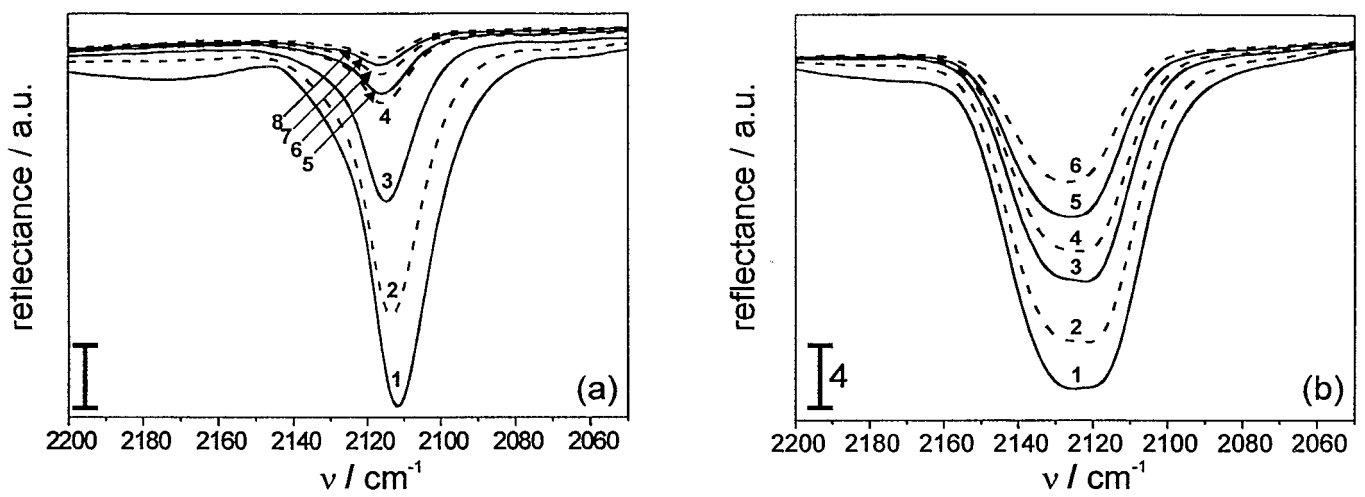

FIG. 8. DRIFT spectra of CO desorbed in an argon stream at room temperature from uncalcined catalysts (5200 ppm CO/He, steady state). (a) Au/TiO_2 after (1) 0, (2) 2, (3) 4, (4) 6, (5) 10, (6) 16, (7) 28, and (8) 40 min. (b) Au/ZrO_2 after (1) 0, (2) 2, (3) 4, (4) 6, (5) 10, and (6) 20 min.

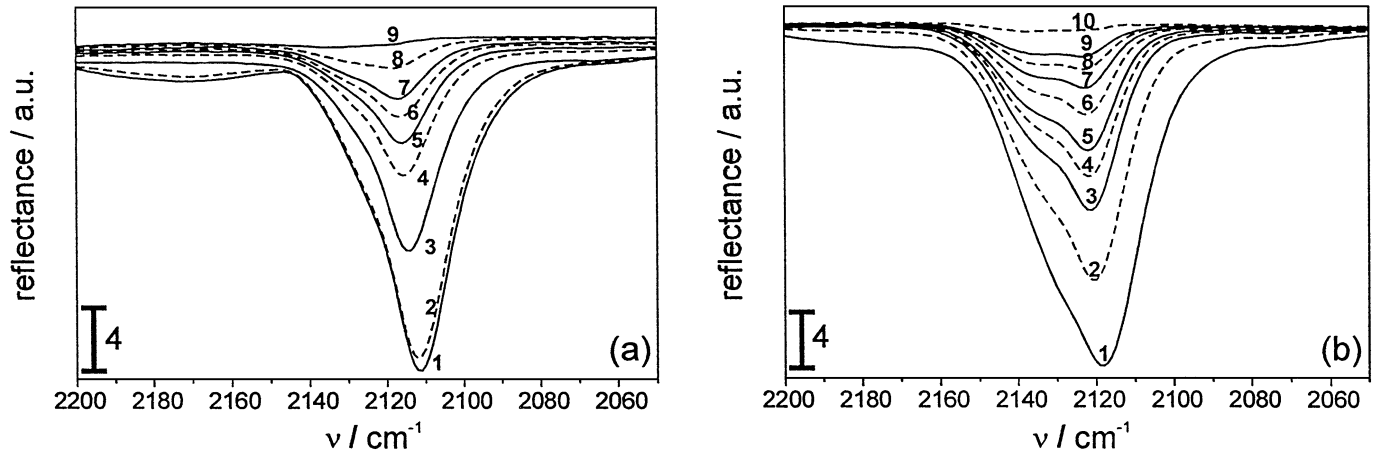

FIG. 9. DRIFT spectra of CO desorption at room temperature from calcined catalysts after their use in CO oxidation (switch from 5200 ppm CO/He to Ar). (a) Au/TiO_2 after (1) 2, (2) 4, (3) 6, (4) 8, (5) 10, (6) 12, (7) 14, (8) 18, and (9) 24 min. (b) Au/ZrO_2 after (1) 2, (2) 4, (3) 6, (4) 8, (5) 10, (6) 14, (7) 18, (8) 22, (9) 28, and (10) 34 min.

decreased steadily. It was much more pronounced for Au/TiO_2 than for Au/ZrO_2. Note that these catalysts did not have a significant initial catalytic activity at room temperature in the DRIFTS cell.

3.3.3. CO desorption into O_2 stream (reaction of pre-adsorbed CO with O_2). CO was adsorbed on uncalcined and *ex situ* calcined Au/TiO_2 and Au/ZrO_2 catalysts and thereafter exposed to flowing O_2 instead of Ar in order to draw conclusions concerning their activity at room temperature and to gain further insight into the properties of the reactive centres. DRIFTS spectra are shown in Figs. 11 (uncalcined catalysts) and 12 (calcined catalysts).

With an uncalcined Au/TiO_2 catalyst, a small band due to free CO_2 appeared (Fig. 11a), the band of adsorbed CO shifted from 2112 to 2115 cm^{-1}, and the CO disappeared much more quickly than in Ar due to reaction. Applying the same procedure on the uncalcined zirconia-based catalyst, negligible amounts of CO_2 were formed (Fig. 11b) and the decrease of the adsorbed CO band intensities was similar to that observed in Ar (Fig. 8b).

The "used catalysts," however, showed a much quicker desorption (Figs. 12a and 12b) by reaction with O_2. Bands of free CO_2 were discernible and more intense with Au/TiO_2 than with Au/ZrO_2. Location of the carbonyl stretching bands at 2111–2115 cm^{-1} (Au/TiO_2) and 2118–2123 cm^{-1} (Au/ZrO_2) were similar to those observed for desorption in Ar and showed a similar frequency shift.

3.3.4. Measurements under reaction conditions. DRIFTS spectra of calcined catalysts were recorded after exposure to 2500 ppm CO in He until steady state was reached; then the gas stream was changed to 2500 ppm CO and 2500 ppm O_2 in He (Fig. 13). These conditions were

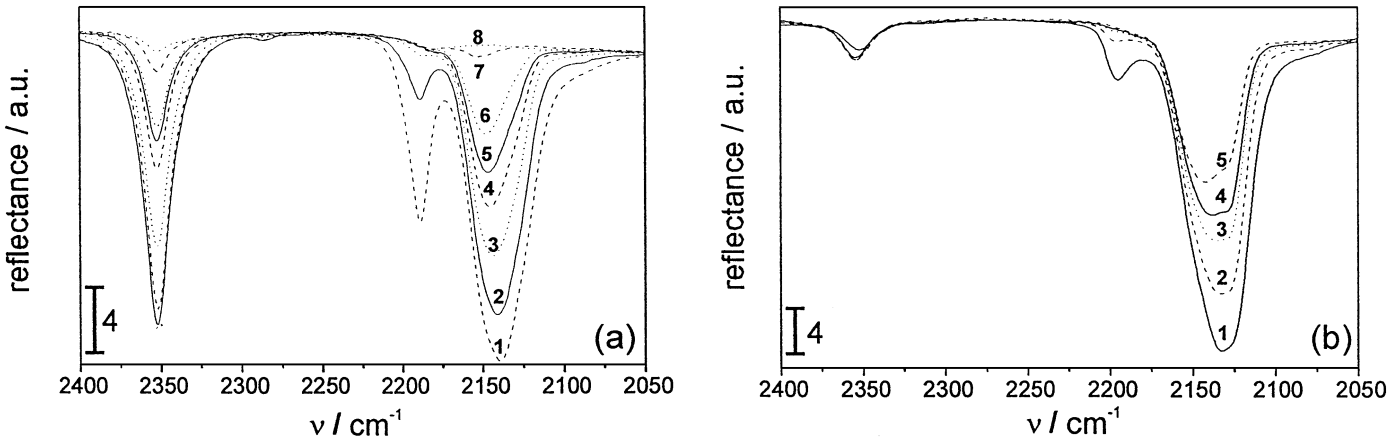

FIG. 10. DRIFT spectra of CO desorption after *in situ* oxidation at 573 K and subsequent CO adsorption at 298 K. (a) Au/TiO_2 after (1) 2, (2) 4, (3) 6, (4) 10, (5) 14, (6) 18, (7) 36, and (8) 90 min. (b) Au/ZrO_2 after *in situ* oxidation at 573 K and subsequent CO adsorption at 298 K after (1) 2, (2) 4, (3) 6, (4) 8, and (5) 10 min.

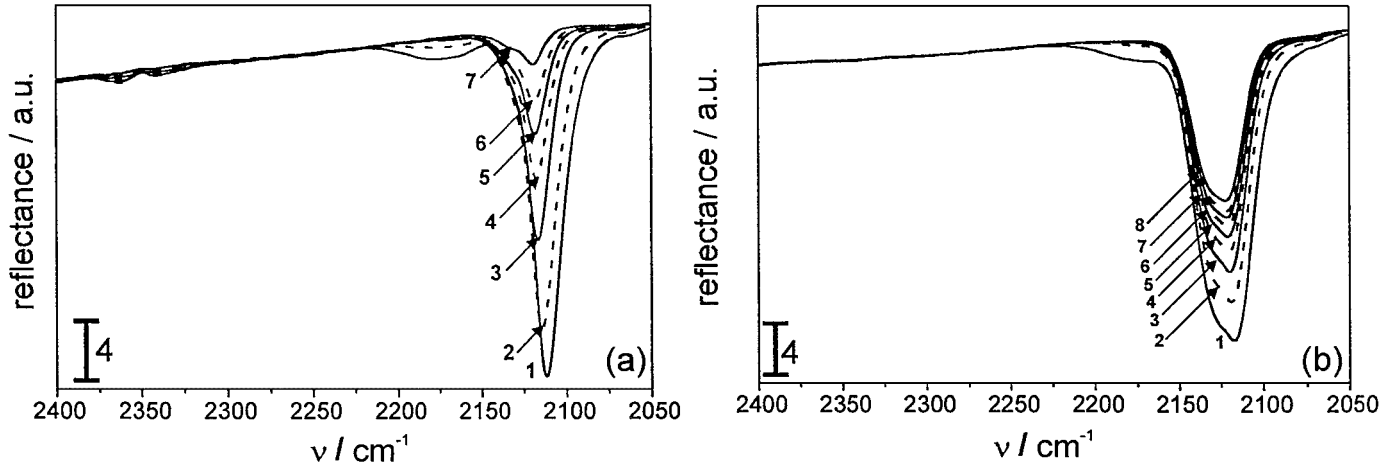

FIG. 11. DRIFT spectra of CO pre-adsorbed on uncalcined catalysts during exposure to an O_2 stream (5000 ppm O_2/He) at room temperature. (a) Au/TiO_2 after (1) 0, (2) 2, (3) 4, (4) 6, (5) 8, (6) 10, and (7) 14 min. (b) Au/ZrO_2 after (1) 0, (2) 2, (3) 4, (4) 6, (5) 8, (6) 10, (7) 14, and (8) 18 min.

very similar to those used during catalytic measurements. During the switch from CO to $CO + O_2$ the band shifted slightly from 2112 to 2117 cm^{-1} with titania supported gold, and from 2118 to 2120 cm^{-1} with zirconia supported gold. The bands of free CO_2 were more intense for Au/TiO_2, indicating again higher activity of the titania-supported catalyst. With Au/ZrO_2 no significant CO_2 formation was detected even at 393 K.

4. DISCUSSION

It is well known that Au clusters of 2.0–3.0 nm show high activity in CO oxidation (3, 8). Using gold colloids instead of previously reported methods like impregnation, deposition–precipitation (2, 3, 6), CVD-methods (17), or fixation of phosphines (4, 15), small gold nanoparticles on metal oxides were produced on TiO_2 and ZrO_2. Since the particle size is nearly preserved during fixation of the gold colloids, the particle size of gold on titania and zirconia is similar. Moreover, surface analysis with XPS revealed that the gold particles are in metallic state. No significant amounts of oxidized species due to insufficient reduction of the precursor $HAuCl_4$ or due to reoxidation in air were found, since there is no shoulder at the Au $4f_{7/2}$ and Au $4f_{5/2}$ peaks, as reported for Au on Fe_2O_3 by Epling *et al.* (26). The content of phosphorous and sodium impurities on the surface, when anchoring at pH 2, was low, as determined by XPS. Additional investigations revealed that the concentration of contaminants was particularly low if the gold deposition was performed in acidic solution, probably because under basic conditions the surface is negatively charged and sodium can be adsorbed by electrostatic interaction.

Catalytic measurements in the microreactor, DRIFTS spectra during CO desorption into oxygen stream or under reaction conditions (band of free CO_2), and thermogravimetric analysis (formation of CO_2 during CO pulse)

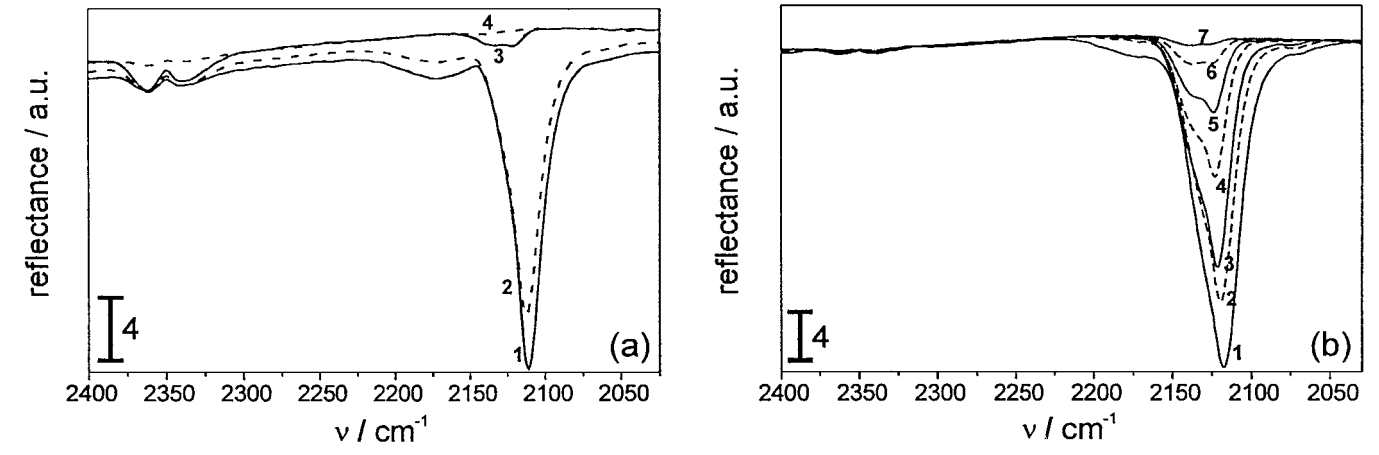

FIG. 12. DRIFT spectra of CO pre-adsorbed on calcined catalysts during exposure to an O_2 stream at room temperature (switch from 5200 ppm CO/He to 5000 ppm O_2/He). (a) Au/TiO_2 after (1) 0, (2) 2, (3) 4, and (4) 6 min. (b) Au/ZrO_2 after (1) 2, (2) 4, (3) 6, (4) 8, (5) 10, (6) 14, and (7) 18 min.

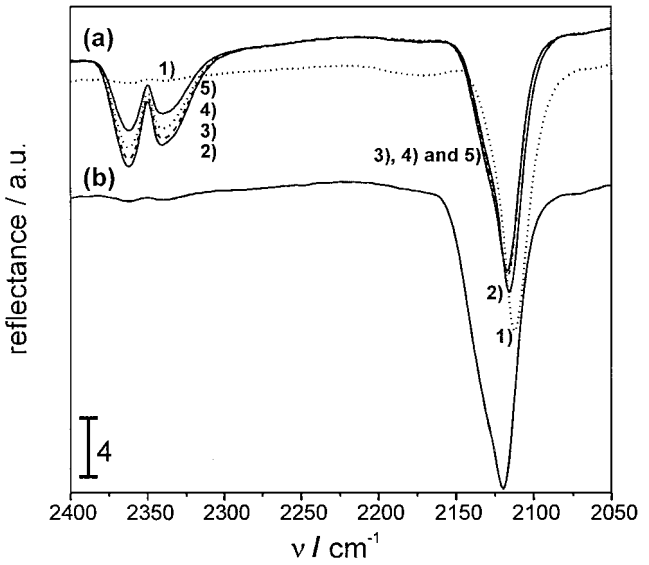

FIG. 13. DRIFT spectra of calcined gold catalysts during change from 2500 ppm CO in He to reaction mixture (2500 ppm CO and 2500 ppm O_2 in He) at room temperature. (a) Au/TiO_2 after (1) 2, (2) 4, (3) 8, (4) 10, and (5) 20 min and at (6) steady state. (b) Au/ZrO_2 at steady state.

showed that the titania-supported gold catalyst is active, even though it was not calcined. This is in contrast to recent results by Tsubota *et al.* (27), who reported that gold particles supported on metal oxides do not display catalytic activity unless heated to very high temperatures.

In contrast to uncalcined Au/TiO_2, the uncalcined Au/ZrO_2 showed no significant activity. Heating Au/ZrO_2 to moderate temperatures did not increase its activity, whereas the activity of Au/TiO_2 increased significantly upon heating the sample in the reaction atmosphere to 420 K (Fig. 6). Following calcination of the gold catalysts at 673 K, the catalytic activity increased significantly, particularly with Au/ZrO_2. The activity of Au/TiO_2 was superior to that of Au/ZrO_2 also after calcination. This behaviour is in line with previous results obtained with corresponding catalyst systems prepared by other methods (compare, e.g., (18) and (3)). According to XPS results the metallic character of gold was maintained. The existence of some broader Au 4*f* peaks indicated (Fig. 2) that some of the particles might have been slightly oxidized, however, to a much lower extent than reported in Ref. (26).

The data gathered in this work indicate that another factor, apart from particle size, may be crucial for catalytic activity. Evidence for this emerges from the fact that the particle size distribution of gold in both systems is similar, whereas catalytic properties are vastly different. In previous publications (33, 34), it was reported that the shape of the particles also plays a significant role. Whereas the particles seem to be spherical directly after anchoring onto the support, there are more significant differences after activation in air. On Au/ZrO_2 some of the gold particles appear with hexagonal shape in the TEM image. As known from earlier studies (35), such particles mainly contain Au(111) faces. With Au/TiO_2 the particles are more spherical, and consequently the contrast in the microscope is much poorer compared to the uncalcined catalyst. There are no fringes evident. In a few cases they were found for Au/ZrO_2. This indicates that the particles are less crystalline, and probably expose more step/kink sites as well as point defects on the surface. The different particle shape after calcination could be due to different interfacial energy of the supports with gold (36) and/or restructuring during heat treatment. Note that only little sintering of gold occurred in both systems upon heat treatment in air, in contrast to results obtained by Valden *et al.* (7, 8). This is probably due to the fact that the surfaces of polycrystalline titania exhibit significantly more defects than a single crystal $TiO_2(110)$ surface. In addition, we did not observe strong particle aggregation of gold particles supported on rough TiO_2 films on Au(111)/mica (systems described in Ref. (12)).

DRIFTS studies were performed in order to further characterize the gold sites existing on the different catalysts and to elucidate the nature of the reversible CO adsorption. In general, the investigation of the gold sites on calcined and uncalcined Au/TiO_2 and Au/ZrO_2 catalysts with CO adsorption in FTIR showed that there are significant differences dependent on the support and the heat treatment of the catalyst. Characteristic bands used for the comparative study are listed in Table 3.

On uncalcined catalysts, two different bands, located at 2110–2120 cm^{-1} and around 2130 cm^{-1}, were found. A band around 2110 cm^{-1} has also been reported on Au(332) (28), and recently on gold particles supported on TiO_2/Mo(100) (37); it is due to adsorption on low-coordinated step/kink defect sites. Adsorption on terrace sites is difficult and normally results in CO vibrations located at lower frequencies. They were not observed in our studies, probably due to the low CO partial pressure.

Desorption from the step/edge sites occurred rather rapidly from both catalysts. This can be attributed to the low adsorption energy of CO on these sites. The initial heat of adsorption on Au(332) and polycrystalline gold is 55–58 kJ/mol (on step sites), whereas it is only 34 kJ/mol on the Au(110) surface (38). Boccuzzi *et al.* (30) and Bollinger and Vannice (2) observed a typical CO band on gold catalysts with small particle size around 2105 cm^{-1}. In our study, the bands are shifted to higher wavenumbers (2110–2120 cm^{-1}), because of the lower CO partial pressure. Such a "blue shift" of the CO band at lower coverages was previously described in Ref. (39). In line with this we also observed a shift in energy during desorption of CO or when using different CO partial pressures.

Comparing Au on titania and zirconia, it emerges that the CO absorption bands are shifted to higher frequencies

for the step/edge gold sites for Au/ZrO_2. The desorption of CO proceeds more slowly, indicating stronger adsorption of CO on zirconia than on titania-supported gold particles. Additionally, the shoulder around 2130 cm^{-1} is much more pronounced for Au/ZrO_2 compared to Au/TiO_2. This band is probably due to CO adsorption on positively polarized gold species, as also observed by Chang *et al.* (40) on gold electrodes, and Boccuzzi *et al.* (41) on gold catalysts.

Desorption into an oxygen stream supported that CO is bonded more strongly on gold particles deposited on zirconia (Figs. 11 and 12) and does not react so quickly with oxygen from the ambient atmosphere. This all indicates that there are different gold sites in Au/TiO_2 and Au/ZrO_2 which cannot be traced alone to a particle size effect.

The fact that on Au/TiO_2 the CO bands for step/edge sites (2110–2120 cm^{-1}) are more prominent than on Au/ZrO_2 suggests that those sites could be responsible for CO oxidation. It can be speculated that the positively polarized gold sites (around 2130 cm^{-1}) do not play a crucial role in CO oxidation. This can be inferred from the fact that the less active catalyst Au/ZrO_2 shows considerably higher intensity of this band.

Interestingly, an *in situ* treatment of the catalyst in air (with cooling in air) led to a temporarily inactive catalyst, where CO was bound more strongly on positively polarized gold sites on both catalysts (2130–2140 cm^{-1}). There is no contribution from step or kink sites (no adsorption below 2120 cm^{-1}), supporting the hypothesis that those low-coordinated gold sites are responsible for the oxidation of CO. Instead there is a band around 2354 cm^{-1}, which can be assigned to adsorbed CO_2. This band has also been reported in previous studies on gold electrodes (32). The Au/TiO_2 catalyst regained its activity more rapidly, showing that a possible restructuring caused by the treatment in oxygen is more stable for Au/ZrO_2. From recent surface science studies it emerges that Au(111) can undergo a stable restructuring in air (42). Such restructuring could temporarily inhibit the reaction after calcination in air.

To sum up, the comparative electronmicroscopy and DRIFTS studies of Au/ZrO_2 and Au/TiO_2 show that the gold particle size is similar on both catalysts, whereas the exposed gold sites are different, depending on support and activation treatment. Valden *et al.* (7, 8) found in a model catalyst study that the optimum size for gold particles is around 2.5 nm, and they explained it by a quantum size effect. A similar optimum for the particle size has previously been found by Haruta *et al.* (43).

The number of kink/step sites is expected to change with the gold particle size: the smaller the particle size, the more step/kink sites will be present on the surface. Only if two-dimensional islands develop at very low coverage will their number decrease again. Since CO is bound reversibly on gold in all systems and weakly on the most active catalysts, CO adsorption is unlikely to be the crucial step for CO oxidation, as already concluded in a previous model catalyst study (12). The better activity could be explained by the fact that oxygen is activated on the support or interface and has to migrate to active centres on the gold particles (10, 12). However, there have to be centres on the gold surface that are able to adsorb oxygen. Oxygen adsorption does not occur on gold single-crystal surfaces, and an activation barrier exists for dissociative O_2 adsorption (44, 45). Hence, terrace sites are probably not able to adsorb CO and oxygen at the same time. This role could be fulfilled by kink or step sites, because adsorption energies are higher on these than on terrace sites, as theoretically calculated for several examples by the Nørskov group (46).

5. CONCLUSIONS

Structural and catalytic properties in CO oxidation have been compared for gold particles deposited on titania and zirconia. The gold particles on both supports are in a metallic state, as evidenced by XPS. The particles of about 2 nm in size, as indicated by HRTEM and XRD, are stable during calcination in air. The catalytic activity in low-temperature CO oxidation was found to depend on support and calcination procedure, in line with previous results, where Au/TiO_2 and Au/ZrO_2 catalysts were prepared with different procedures (3, 18, 47). From the detailed investigation with DRIFTS, in addition to structural analysis with HRTEM, we conclude that the number of low-coordinated gold sites is different on the two supports due to different support interactions resulting in different shapes of the gold particles. Calcination affects the number of low-coordinated gold sites, which are suggested to be responsible for the adsorption of oxygen and carbon monoxide, because terrace sites are not able to adsorb oxygen according to single-crystal studies and theoretical calculations. However, further model catalyst studies and calculations are needed to substantiate this hypothesis.

ACKNOWLEDGMENT

Thanks are due to C. Wögerbauer for performing measurements of CO conversion on the gold catalysts.

REFERENCES

1. Outka, D. A., and Madix, R. J., *Surf. Sci.* **179**, 351 (1987).
2. Bollinger, M. A., and Vannice, M. A., *Appl. Catal. B Environ.* **8**, 417 (1996).
3. Haruta, M., Tsubota, S., Kobayashi, T., Kageyama, H., Genet, M. J., and Delmon, B., *J. Catal.* **144**, 175 (1993).
4. Yuan, Y. Z., Kozlova, A. P., Asakura, K., Wan, H., Tsai, K., and Iwasawa, Y., *J. Catal.* **170**, 191 (1997).
5. Grunwaldt, J.-D., Kiener, C., Woegerbauer, C., and Baiker, A., *J. Catal.* **181**, 223 (1999).
6. Haruta, M., Yamada, N., Kobayashi, T., and Iijima, S., *J. Catal.* **115**, 301 (1989).

7. Valden, M., Pak, S., Lai, X., and Goodman, D. W., *Catal. Lett.* **56**, 7 (1998).
8. Valden, M., Lai, X., and Goodman, D. W., *Science* **281**, 1647 (1998).
9. Haruta, M., *Catal. Surv. Jap.* **1**, 61 (1997).
10. Haruta, M., *Catal. Today* **36**, 153 (1997).
11. Baiker, A., Grunwaldt, J.-D., Müller, C. A., and Schmid, L., *Chimia* **52**, 517 (1998).
12. Grunwaldt, J.-D., and Baiker, A., *J. Phys. Chem. B* **103**, 1002 (1999).
13. Grunwaldt, J. D., Göbel, U., and Baiker, A., *Fresenius J. Anal. Chem.* **358**, 96 (1997).
14. Grunwaldt, J.-D., Becker, O., and Baiker, A., *in* "Proceedings, 14th International Congress on Electron Microscopy, Cancun, Mexico," Vol. II, p. 431, 1998.
15. Yuan, Y. Z., Asakura, K., Wan, H. L., Tsai, K., and Iwasawa, Y., *Catal. Lett.* **42**, 15 (1996).
16. Visco, A. M., Donato, A., Milone, C., and Galvagno, S., *React. Kinet. Catal. Lett.* **61**, 219 (1997).
17. Okumara, M., Nakamura, S.-I., Tsubota, S., Nakamura, T., and Haruta, M., *Stud. Surf. Sci. Catal.* **118**, 227 (1998).
18. Knell, A., Barnickel, P., Baiker, A., and Wokaun, A., *J. Catal.* **137**, 306 (1992).
19. Briggs, D., and Seah, M. P., "Practical Surface Analysis by Auger and X-Ray Photoelectron Spectroscopy." Wiley, Chichester, 1983.
20. Shirley, D. A., *Phys. Rev. B* **5**, 4709 (1972).
21. Maciejewski, M., and Baiker, A., *Thermochim. Acta* **295**, 95 (1997).
22. Maciejewski, M., Müller, C. A., Tschan, R., Emmerich, W. D., and Baiker, A., *Thermochim. Acta* **295**, 167 (1997).
23. Gregg, S. J., and Wing, K. S. W., *Surf. Colloid. Sci.* **9**, 254 (1976).
24. Buffat, P., and Borel, J.-P., *Phys. Rev. A* **13**, 2287 (1976).
25. Pireaux, J. J., Liehr, M., Thiry, P. A., Delrue, J. P., and Caudano, R., *Surf. Sci.* **141**, 221 (1984).
26. Epling, W. S., Hoflund, G. B., Weaver, J. F., Tsubota, S., and Haruta, M., *J. Phys. Chem. B* **100**, 9929 (1996).
27. Tsubota, S., Nakamura, T., Tanaka, K., and Haruta, M., *Catal. Lett.* **56**, 131 (1998).
28. Ruggiero, C., and Hollins, P., *Surf. Sci.* **377**, 583 (1997).
29. Tadayyoni, M. A., and Weaver, M. J., *Langmuir* **2**, 179 (1986).
30. Boccuzzi, F., Chiorino, A., Tsubota, S., and Haruta, M., *J. Phys. Chem. B* **100**, 3625 (1996).
31. Tsyganenko, A. A., Denisenko, L. A., Zverev, S. M., and Filimonov, V. N., *J. Catal.* **94**, 10 (1985).
32. Chang, S. C., Hamelin, A., and Weaver, M. J., *Surf. Sci. Lett.* **239**, 543 (1990).
33. Vogel, W., Cunningham, D. A. H., Tanaka, K., and Haruta, M., *Catal. Lett.* **40**, 175 (1996).
34. Cunningham, D. A. H., Vogel, W., Kageyama, H., Tsubota, S., and Haruta, M., *J. Catal.* **177**, 1 (1998).
35. Perez-Alvarez, M., Ascencio, J. A., Gutierrez-Wing, C., and Jose-Yacaman, M., *in* "Proceedings 14th International Congress on Electron Microscopy, Cancun, Mexico," Vol. II, p. 459, 1998.
36. Campbell, C. T., *Surf. Sci. Rep.* **27**, 1 (1997).
37. Rainer, D. R., Xu, C., Holmblad, P. M., and Goodman, D. W., *J. Vac. Sci. Technol. A* **15**, 1653 (1997).
38. Ruggiero, C., and Hollins, P., *J. Chem. Soc. Faraday Trans.* **92**, 4829 (1996).
39. Hollins, P., *Surf. Sci. Rep.* **16**, 52 (1992).
40. Chang, S. C., Hamelin, A., and Weaver, M. J., *J. Phys. Chem. B* **95**, 5560 (1991).
41. Boccuzzi, F., Chiorino, A., Tsubota, S., and Haruta, M., *Catal. Lett.* **29**, 225 (1994).
42. Chevrier, J., Huang, L., Zeppenfeld, P., and Comsa, G., *Surf. Sci.* **352–354**, 285 (1996).
43. Baumweda, G. R., Tsubota, S., Nakamura, T., and Haruta, M., *Catal. Lett.* **44**, 83 (1997).
44. Canning, N. D. S., Outka, D., and Madix, R. J., *Surf. Sci.* **141**, 240 (1984).
45. Skelton, D. C., Tobin, R. G., Lambert, D. K., DiMaggio, C. L., and Fisher, G. B., *J. Phys. Chem. B* **103**, 964 (1999).
46. Hammer, B., and Norskov, J. K., *in* "Chemisorption and Reactivity on Supported Clusters and Thin Films" (R. M. Lambert and G. Pacchioni, Eds.), p. 285. Kluwer Academic, Dordrecht, 1997.
47. Boccuzzi, F., Cerrato, G., Pinna, F., and Strukul, G., *J. Phys. Chem. B* **102**, 5733 (1998).